ADVANCED MATERIALS

(10:1, 55 nm) and was deposited by the co-evaporation of magnesium and silver metals, with deposition rates of 5 and 0.5 Å s^{-1}, respectively. The other was LiF/Al and was deposited by first evaporating LiF (0.5 nm) at a deposition rate of 0.1 Å s^{-1} and then evaporating aluminum (400 nm) at a rate of 1–2 Å s^{-1}. The cathode was then capped with silver metal (100 nm) by evaporating silver at a rate of 3 Å s^{-1}. The effective area of the emitting diode was 9.00 mm^2. Current, voltage, and light-intensity measurements were made simultaneously using a Keithley 2400 source meter and a Newport 1835-C optical meter equipped with a Newport 818-ST silicon photodiode. All chemicals used for EL devices were sublimed in vacuum prior to use.

Received: September 11, 2002

[1] a) M. A. Baldo, D. F. O'Brien, Y. You, A. Shoustikov, S. Sibley, M. E. Thompson, S. R. Forrest, *Nature* **1998**, *395*, 151. b) D. F. O'Brien, M. A. Baldo, M. E. Thompson, S. R. Forrest, *Appl. Phys. Lett.* **1999**, *74*, 442.

[2] a) R. C. Kwong, S. Sibley, T. Dubovoy, M. Baldo, S. R. Forrest, M. E. Thompson, *Chem. Mater.* **1999**, *11*, 3709. b) W. Lu, B. X. Mi, M. C. W. Chan, Z. Hui, N. Zhu, S. T. Lee, C. M. Che, *Chem. Commun.* **2002**, 206.

[3] a) Y. G. Ma, H. Y. Zhang, J. C. Shen, C. M. Che, *Synth. Met.* **1998**, *94*, 245. b) X. Z. Jiang, A. K. Y. Jen, B. Carlson, L. R. Dalton, *Appl. Phys. Lett.* **2002**, *80*, 713.

[4] a) V. V. Grushin, N. Herron, D. D. LeCloux, W. J. Marshall, V. A. Petrov, Y. Wang, *Chem. Commun.* **2001**, 1494. b) H. Z. Xie, M. W. Liu, O. Y. Wang, X. H. Zhang, C. S. Lee, L. S. Hung, S. T. Lee, P. F. Teng, H. L. Kwong, H. Zheng, C. M. Che, *Adv. Mater.* **2001**, *13*, 1245. c) S. Lamansky, P. Djurovich, D. Murphy, F. Abdel-Razzaq, H. E. Lee, C. Adachi, P. E. Burrows, S. R. Forrest, M. E. Thompson, *J. Am. Chem. Soc.* **2001**, *123*, 4304.

[5] a) Y. Wang, N. Herron, V. V. Grushin, D. LeCloux, V. Petrov, *Appl. Phys. Lett.* **2001**, *79*, 449. b) J. P. J. Markham, S. C. Lo, S. W. Magennis, P. L. Burn, I. D. W. Samuel, *Appl. Phys. Lett.* **2002**, *80*, 2645. c) J. C. Ostrowski, M. R. Robinson, A. J. Heeger, G. C. Bazan, *Chem. Commun.* **2002**, 784.

[6] a) M. A. Baldo, S. Lamansky, P. E. Burrows, M. E. Thompson, S. R. Forrest, *Appl. Phys. Lett.* **1999**, *75*, 4. b) C. Adachi, M. A. Baldo, S. R. Forrest, M. E. Thompson, *Appl. Phys. Lett.* **2000**, *77*, 904. c) M. Ikai, S. Tokito, Y. Sakamoto, T. Suzuki, Y. Taga, *Appl. Phys. Lett.* **2001**, *79*, 156. d) C. Adachi, M. A. Baldo, M. E. Thompson, S. R. Forrest, *J. Appl. Phys.* **2001**, *90*, 5048.

[7] a) C. Adachi, M. A. Baldo, S. R. Forrest, S. Lamansky, M. E. Thompson, R. C. Kwong, *Appl. Phys. Lett.* **2001**, *78*, 1622. b) R. C. Kwong, M. R. Nugent, L. Michalski, T. Ngo, K. Rajan, Y. J. Tung, M. S. Weaver, T. X. Zhou, M. Hack, M. E. Thompson, S. R. Forrest, J. J. Brown, *Appl. Phys. Lett.* **2002**, *81*, 162. c) B. W. D'Andrade, M. E. Thompson, S. R. Forrest, *Adv. Mater.* **2002**, *14*, 147.

[8] D. M. Hall, H. Y. Hwang, B. Bhanthumnavin, *J. Chem. Soc., Perkin Trans 2* **1973**, 2131.

[9] C. W. Ko, Y. T. Tao, J. T. Lin, K. R. J. Thomas, *Chem. Mater.* **2002**, *14*, 357.

Nanobelts, Nanocombs, and Nanowindmills of Wurtzite ZnS**

By *Christopher Ma*, *Daniel Moore*, *Jing Li*, and *Zhong L. Wang**

Zinc sulfide has received great attention in recent years for its potential applications in optoelectronics.[1–3] This wide bandgap semiconductor[4] has a high refractive index[3] and a high transmittance in the visible range.[5,6] As the current research is driving toward nanoscale phenomena and technology, the synthesis of ZnS nanomaterials is of great interest. Quasi-one-dimensional nanostructures of ZnS are attractive because they are candidates for fabricating electronic and optoelectronic nanodevices.[7,8]

Zinc sulfide has two types of crystal structures: hexagonal wurtzite ZnS (referred to as the hexagonal phase) and cubic zinc blende ZnS (referred to cubic phase). Typically, the stable structure at room temperature is zinc blende, with few observances of stable wurtzite ZnS.[9–12] There are a couple of reports about nanowire structures of ZnS. Using a reverse micelle solution-based technique, Wu et al. have fabricated zinc blende structured ZnS nanowires.[13] Based on ZnO nanorods and nanobelts made by a physical process, Dloczik et al. and Wang et al. have, respectively, converted ZnO into zinc blende-structured ZnS nanorods and nanotubes that have porous structures made of nanocrystallites with grain sizes of ~7 nm.[14,15]

In this paper, we report the success of synthesizing stable wurtzite-structured nanobelts, nanocombs, and nanowindmills using a simple catalyst-free thermal evaporation technique. The structures of these characteristic shapes have been fully characterized. Detailed study on the phase transformation from wurtzite to zinc blende is presented. It is anticipated that these novel structures will have some unique applications in nanophotonics.

Our synthesis technique is based on thermal evaporation of ZnS powders at elevated temperatures. The as-synthesized sample is composed of several types of structures. The most typical structure observed is ZnS nanobelts (Fig. 1a). The nanobelt morphology has been previously observed for a group of transparent conductive oxides.[16] The nanobelts have a uniform cross-section along their length, with a typical width of 2–30 μm, and extend to over 100 μm in length. The growth

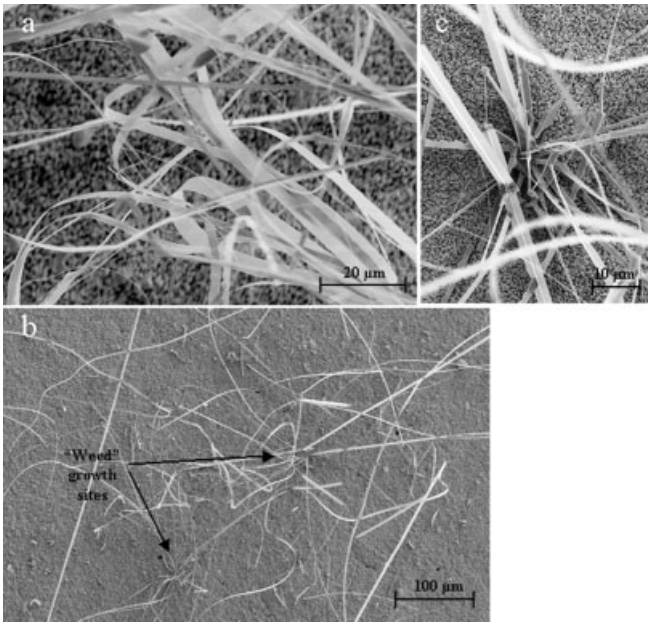

Fig. 1. a) SEM image of ZnS nanobelts and nanosaws grown from an alumina substrate. b,c) Distribution of the ZnS nanobelts on the substrate surface suggesting a "weed growth" model.

[*] Prof. Z. L. Wang, C. Ma, D. Moore, Dr. J. Li
Center for Nanoscience and Nanotechnology
School of Materials Science and Engineering
Georgia Institute of Technology
Atlanta, GA 30332-0245 (USA)
E-mail: zhong.wang@mse.gatech.edu

[**] Research sponsored by MDI N00014-95-1-1116 for the Office of Naval Research, NSF, and NASA.

 © 2003 WILEY-VCH Verlag GmbH & Co. KGaA, Weinheim 0935-9648/03/0302-0228 $ 17.50+.50/0

of the nanobelts does not show any specific pattern, rather they are nucleated and grown as bunches randomly distributed on the substrate covered by a thin layer of ZnS film. This is referred to be the "weed growth" model (Fig. 1b). A closer examination at the root of the bunch shows that the nanobelts were grown from a site, which is believed to be the "seed" for the nucleation of the nanobelts (Fig. 1c). Numerous belt- and saw-like structures grow from a single nucleation site.

Several other types of shapes have also been identified. The comb-like structure is found in the product (Fig. 2a), and large sheets have also been identified (Fig. 2b). These structures are single-crystalline. Shrinkage in thickness significantly increases their flexibility, thus the structure remains intact even after folding back. This sheet-type structure has previously observed for Ga_2O_3 and CdO.[16,17]

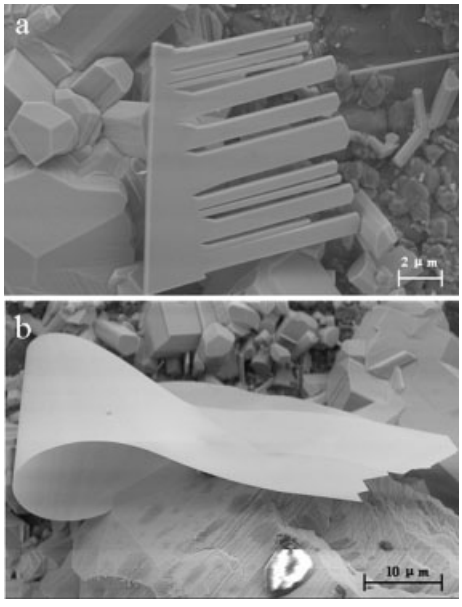

Fig. 2. SEM images of ZnS comb-like and sheet-like structures.

Electron diffraction and X-ray diffraction (XRD) techniques have been used to determine the crystal structure of the ZnS nanostructures. An effort to characterize the structures by XRD alone was made. The samples appear to have a wurtzite structure, but wurtzite peaks and sphalerite peaks are indistinguishable from each other. This makes it unfeasible to determine the structure of the zinc sulfide from the XRD pattern alone.

Our systematic analysis using electron diffraction indicates that all three types of structures are single-crystalline with the wurtzite ZnS structure ($a = 3.82$ Å, $c = 6.26$ Å). The comb-like, saw-toothed belts, and the regular belt structures were found in the same growth temperature range. Bright-field transmission electron microscopy (TEM) images of these structures are shown in Figure 3. No particle was observed at the ends of any of the structures. The ripple-like contrast observed in the TEM images is due to the strain resulting from the bending of the nanobelts. The growth characteristics of these structures show some consistency. Shown in Figure 3a is a TEM image

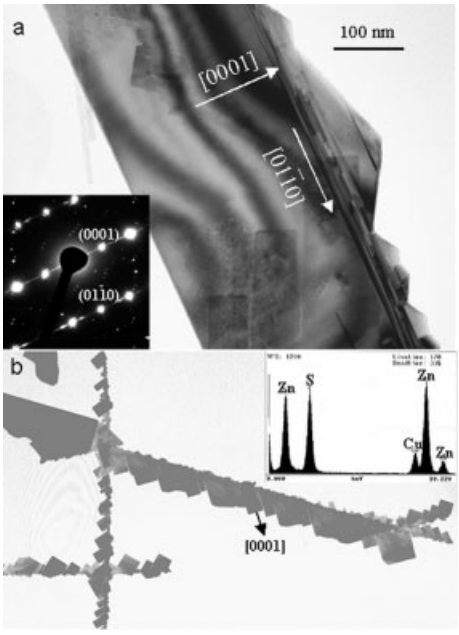

Fig. 3. a) TEM image and the corresponding electron diffraction pattern from a belt- and saw-like ZnS structure. b) TEM image of the comb-like ZnS nanostructure. The inset is an EDS (energy-dispersive X-ray spectroscopy) spectrum showing the existence of sulfur and zinc atoms in the specimen, while the Cu signal came from the TEM grid used for supporting the sample.

of a ZnS nanobelt with one side having the saw-tooth structure is shown. The nanobelt grows along [0001], with side surfaces (01$\bar{1}$0) and the top surfaces (2$\bar{1}\bar{1}$0). The extrusive sawteeth point along [01$\bar{1}$0], and their top surfaces are (2$\bar{1}\bar{1}$0). The sawteeth are defined by facets close to (01$\bar{1}$3) and (0$\bar{1}$13). A common feature observed is that (0001) stacking faults are usually present between the teeth and the nanobelt. The comb-like fingertip structure is formed by the formation of low-energy facets of (0001) and (01$\bar{1}$0), while the top surfaces are still (2$\bar{1}\bar{1}$0). The fingers for the comb-like structures are pointing toward [0001]. Our study shows that the two fastest growth directions for ZnS are [0001] and [0$\bar{1}\bar{1}$0], and the largest facets are (2$\bar{1}\bar{1}$0).

Another structure observed is the six-fold windmill structure (Fig. 4a), in which the axis is [0001] and the six wings are along ±[10$\bar{1}$0], ±[0$\bar{1}$10], and ±[$\bar{1}$100], as shown schematically in Figure 4c. This type of structure has been previously observed for hexagonal ZnO.[18,19] The six wings can grow laterally and interconnect to form a faceted structure like the one shown in Figure 4b, where the side facets are likely to be (10$\bar{1}$1), ($\bar{1}$011), (01$\bar{1}$1), (0$\bar{1}$11), ($\bar{1}$101), and (1$\bar{1}$01). This type of faceted three-dimensional polyhedral structure is fairly common in the synthesized material.

As we pointed out at the beginning, wurtzite-structured ZnS is unstable and it may transform to zinc blende structure. Shown in Figures 5a and b are two images recorded from the same area before and after the sample was illuminated for about 10 min under 200 kV electrons, showing an increase in the density of planar defects. The electron diffraction pattern recorded from the area shows the coexistence of the hexago-

 © 2003 WILEY-VCH Verlag GmbH & Co. KGaA, Weinheim 0935-9648/03/0302-0229 $ 17.50+.50/0

ADVANCED MATERIALS

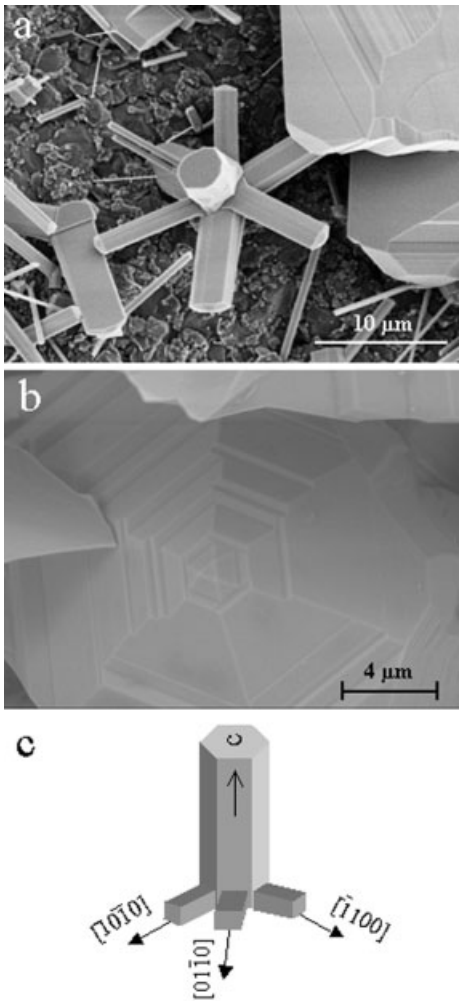

Fig. 4. a) SEM image of the windmill structure. b) SEM image of the polyhedral structure of ZnS. c) Structural model of the windmill structure.

nal wurtzite structure and the cubic zinc blende structure (Fig. 5c). The orientation relationships between the two phases are: $[2\bar{1}\bar{1}0]\|[01\bar{1}]$, and $(0001)\|(111)$. The two phases coexist by sharing the same (0001) or (111) plane. It is also known that the cubic phase of ZnS typically has the {111} twins. The existence of the twins is indicated by the electron diffraction pattern. The diffraction spots and the corresponding indexes from the hexagonal phase, the cubic phase and its twin are illustrated in Figure 5d.

Unit-cell models for the hexagonal and cubic phases of ZnS are shown in Figure 6a. The presence of the two phases in the nanobelts can be directly identified by high-resolution TEM. Figure 6b shows a TEM image recorded from the hexagonal phase that is oriented along $[2\bar{1}\bar{1}0]$, which matches fairly well to the projected position of the Zn atoms in the unit cell, as shown in the inset. The sulfur atoms are too light to be resolved by the TEM used for this study. Figure 6c is a $[01\bar{1}]$ projected image of the cubic phase and the projection of the unit cell is marked by a rectangular frame. The projected positions of the Zn atoms in the cubic phase, as shown in the inset, match well to the bright contrast observed in the image.

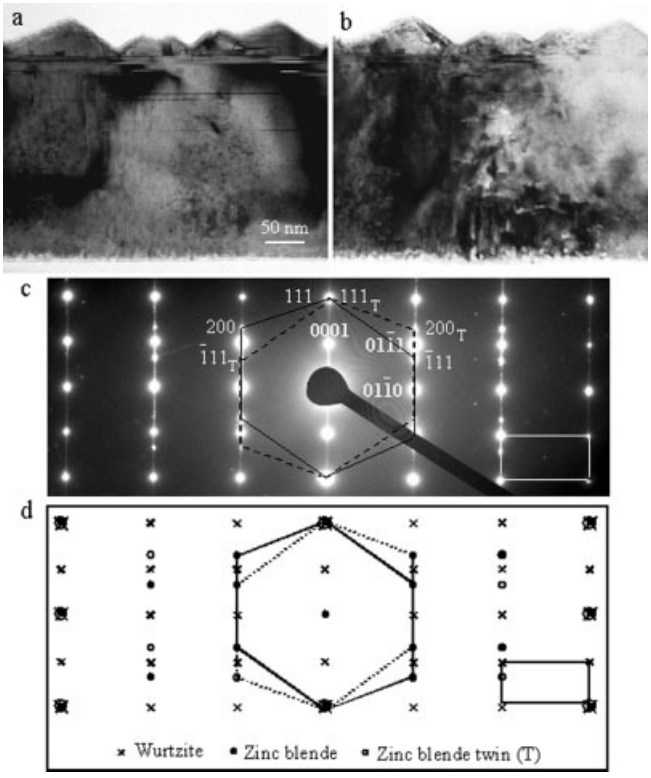

Fig. 5. a,b) TEM images of a saw-like ZnS nanostructure prior and after illumination by an electron beam for ca. 10 min, showing the formation of planar defects. c) Electron diffraction pattern recorded from the area which can be indexed as the coexistence of the hexagonal and cubic phases with the presence of twins in the cubic phase. d) A schematic showing the systematic reflections in corresponding to the experimental pattern shown in (c).

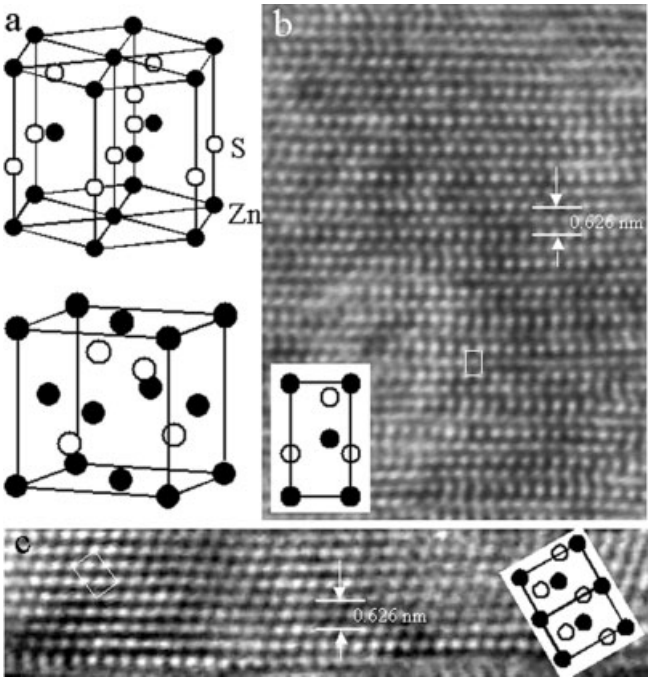

Fig. 6. a) Unit-cell models for the hexagonal and cubic phases. b) $[2\bar{1}\bar{1}0]$ High-resolution TEM image of the wurtzite ZnS. c) $[01\bar{1}]$ High-resolution TEM image of the zinc blende ZnS. The insets are the projections of the corresponding unit cells.

 © 2003 WILEY-VCH Verlag GmbH & Co. KGaA, Weinheim 0935-9648/03/0302-0230 $ 17.50+.50/0

The cubic phase of ZnS can be viewed as being composed of a face-centered cubic (fcc) Zn sublattice with a fcc S sublattice that has been displaced by 1/4 in the [111]-axis direction with respect to the Zn sublattice. From the structural point of view, a face-centered cubic phase is related to a hexagonal close-packed phase by changing the stacking sequence in parallel to the (111) or (0001) plane. For close-packed configurations, there are three distinct stacking layers, named A, B, and C, each of which is composed of one layer of Zn atoms and one layer of S atoms. A stacking of ABAB forms the hexagonal phase, while a stacking of ABCABC forms the cubic phase. The two structures can be transformed simply by changing the stacking sequence. Figure 7 shows a high-resolution TEM image from an area in which the hexagonal and

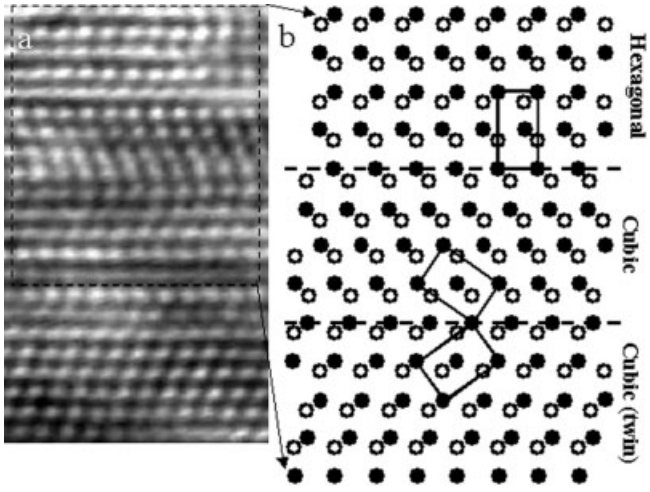

Fig. 7. High-resolution TEM image showing the coexistence of the wurtzite, zinc blende, and the twinned zinc-blend structures; the corresponding structure model is illustrated at the right-hand side showing the transformation among the structures by adjusting the stacking sequence of the atomic layers.

cubic phases coexist; the corresponding structure model for the image is illustrated at the right-hand side in the frame. The incident beam direction is $[2\bar{1}\bar{1}0]$ or $[01\bar{1}]$ for the hexagonal or cubic phase, respectively. The (0001) or (111) plane is the stacking plane. Although the positions of the S atoms cannot be determined from the image, the projected positions of the Zn atoms can be directly provided. The region is composed of two phases and a twin of the cubic phase. The orientation relationship provided by this image matches exactly to that derived from the electron diffraction pattern given in Figure 5c.

In summary, nanostructures of wurtzite-structured ZnS (which is unlikely to be stable under conventional conditions for the bulk), have been synthesized by a simple physical process. Morphologies with belt-, saw-, comb-, and windmill-like nanostructures have been observed. These structures are formed by adjusting the growth directions between [0001] and $\langle 01\bar{1}0\rangle$, and the sizes of the (0001), $(01\bar{1}0)$, and $(2\bar{1}\bar{1}0)$ facets. Electron diffraction and high-resolution TEM have revealed the phase transformation between the hexagonal and cubic phases and their orientation relationship as well as the presence of stacking fault and twins. The unique wurtzite ZnS nanostructures reported here are likely to be useful for optoelectronic devices, and the technique shown here can be an effective approach for the synthesis of ZnS nanostructures.

Experimental

Synthesis of the zinc sulfide nanostructures was carried out by using simple thermal evaporation of a zinc sulfide source powder (purity: 99.9 %) in a horizontal tube furnace. The detailed introduction of the apparatus has been published previously [16]. The source powder was placed in an alumina boat and the boat was placed in the center of the tube furnace. The tube was evacuated for several hours to purge O_2 from the system. The temperature of the system was then raised to 1050 °C at a heating rate of 20 °C min^{-1} and held there at a constant pressure of 300 mbar for 1 h. A steady flow of argon gas was sent through the tube, which acted as a carrier gas to transport the zinc sulfide vapor to cooler temperature zones, where it might deposit onto alumina substrates downstream of the source material.

The as-deposited material was characterized and analyzed by scanning electron microscopy (SEM; LEO 1530 FEG), transmission electron microscopy (TEM; Hitachi HF-2000 FEG at 200 kV, JEOL 4000EX at 400 kV), and energy-dispersive X-ray spectroscopy (EDS).

Received: October 23, 2002
Final version: November 21, 2002

[1] S. Kishimoto, A. Kato, A. Naito, Y. Sakamoto, S. Iida, *Phys. Status Solidi B* **2002**, *1*, 391.
[2] L. Sun, C. Liu, C. Liao, C. Yan, *J. Mater. Chem.* **1999**, *9*, 1655.
[3] X. Jiang, Y. Xie, J. Lu, L. Zhu, W. He, Y. Qian, *Chem. Mater.* **2001**, *13*, 1213.
[4] N. R. Pawaskar, S. D. Sathaye, M. M. Bhadbhade, K. R. Patil, *Mater. Res. Bull.* **2002**, *37*, 1539.
[5] B. Elidrissi, M. Addou, M. Regragui, A. Bougrine, A. Kachouane, J. C. Bernècde, *Mater. Chem. Phys.* **2001**, *68*, 175.
[6] S. Yamaga, A. Yoshikawa, H. Kasai, *J. Cryst. Growth* **1988**, *86*, 252.
[7] S. Gupta, J. C. McClure, V. P. Singh, *Thin Solid Films* **1997**, *299*, 33.
[8] W. Park, J. S. King, C. W. Neff, C. Liddell, C. J. Summers, *Phys. Status Solidi B* **2002**, *2*, 949.
[9] Y. Wang, L. Zhang, C. Liang, G. Wang, X. Peng, *Chem. Phys. Lett.* **2002**, *357*, 314.
[10] S. Takata, T. Minami, T. Miyata, H. Nanto, *J. Cryst. Growth* **1988**, *86*, 257.
[11] Z. P. Qiao, G. Xie, J. Tao, Z. Y. Nie, Y. Z Lin, X. M. Chen, *J. Solid State Chem.* **2002**, *166*, 49.
[12] S.-H. Yu, M. Yoshimura, *Adv. Mater.* **2002**, *14*, 296.
[13] O. Wu, N. Zheng, Y. Ding, Y. Li, *Inorg. Chem. Commun.* **2002**, *5*, 671.
[14] L. Dloczik, R. Engelhardt, K. Ernst, M. Lux-Steiner, R. Könenkamp, *Sens. Actuators B* **2002**, *84*, 33.
[15] X. D. Wang, P. X. Gao, J. Li, C. J. Summers, Z. L. Wang, *Adv. Mater.* **2002**, *14*, 1732.
[16] Z. Pan, Z. Dai, Z. L. Wang, *Science* **2001**, *291*, 1947.
[17] Z. R. Dai, Z. W. Pan, Z. L. Wang, *J. Phys. Chem. B.* **2002**, *106*, 902.
[18] J. Zhang, L. Sun, J. Yin, H. Su, C. Liao, C. Yan, *Chem. Mater.* **2002**, *14*, 4172.
[19] J. Lao, J. Wen, Z. Ren, *Nano Lett.* **2002**, *2*, 1287.

 © 2003 WILEY-VCH Verlag GmbH & Co. KGaA, Weinheim 0935-9648/03/0302-0231 $ 17.50+.50/0